Interrelationships of Nanometer and Subnanometer Structures in a Polynorbornene Containing Second Generation Liquid-Crystalline Monodendrons as Side Groups

Zhen Liu,[†] Lei Zhu,[†] Zhihao Shen,[†] Wensheng Zhou,[†] Stephen Z. D. Cheng,*[,†] Virgil Percec,[‡] and Goran Ungar[§]

Maurice Morton Institute and Department of Polymer Science, The University of Akron, Akron, Ohio 44325-3909; Department of Chemistry, University of Pennsylvania, Philadelphia, Pennsylvania 19104-6323; and Department of Engineering Materials, University of Sheffield, Sheffield S1 3JD, UK

Received June 24, 2002; Revised Manuscript Received September 20, 2002

ABSTRACT: A series of polynorbornenes containing monodendrons as side groups [DPNB(*n*)] with different degrees of polymerization (*n*) were synthesized. These dendritic side groups were second generation monodendrons based on the AB_2 mesogenic monomer, 13-hydroxy-1-(4-hydroxyphenyl)-2-(4-hydroxy-4″-*p*-terphenylyl)tridecane building blocks. Although the mesogens were rodlike, the polymer samples were overall conformationally flexible and displayed liquid-crystalline (LC) behavior. Above $n = 20$ in DPNB(*n*), both the transition temperatures and heats of transitions were independent of *n*. Therefore, a DPNB(40) was chosen as the representative polymer for this study. The polymer exhibited complicated phase transformation behaviors which were associated with two different length scales. During cooling, a nematic (N) phase, two smectic A (S_A and S_A^m) phases, and one hexatic B (S_B^h) phase were observed. Among them, the N phase only appeared in a narrow temperature window of less than 2 °C. The S_A^m phase might be monotropic and metastable with respect to the S_B^h phase. The N phase was formed via the orientation order of the LC mesogens in the monodendrons of the side groups on the subnanometer scale. In addition to the molecular orientation order, both of the S_A and S_A^m phases also possessed the ordered layer structures on the nanometer scale despite different layer spacings (5.35 nm vs 4.90 nm). In the S_B^h phase, the layer structure was much larger than those in both the S_A and the S_A^m phases (8.84 nm), and its lateral molecular packing exhibited a two-dimensional hexagonal array on the subnanometer scale ($a = 0.52$ nm and $\gamma = 120°$). Interrelations of these nanometer and subnamometer structural formations in these phases were discussed.

Introduction

Although the concept of three-dimensional (3D) macromolecules was proposed over half a century ago,[1,2] it was not until the late 1970s that the practical syntheses of dendrimers and hyperbranched polymers were actually prepared.[3−11] Initially, a divergent synthetic approach was used to prepare these polymers. Later, in the 1990s, a convergent synthetic approach was introduced.[12−16] To accelerate the growth, a "double-stage" convergent approach was proposed.[17−19] On the other hand, the uncontrolled chain growth propagation approach was also utilized in synthesizing highly branched polymers.[20,21] In synthesizing these polymers, monodendrons were usually attached to a linear polymeric backbone and then wrapped by an increasing number, from the inner to the outer regions, of wedges of monodendrons. Depending upon the backbone stiffness, the degree of coverage, and the generation (size) of the monodendrons, the overall shape of the hyperbranched polymers in many cases was not spherical but tends to be cylindrical instead.

Two general approaches to design and construct dendritic skeletons exhibiting liquid-crystalline (LC) phases were proposed. The first approach involved attachment of a semirigid dendritic wedge to an ether or a crown ether which functions as an endo receptor. The monodendron itself did not possess the mesogens but acts as self-assemblages to generate tubular architecture, the building block to constructing columnar or cubic structures on the nanometer scale as supramolecular structures.[22−26] The second approach was to directly introduce rodlike mesogens into the monodendrons which were built by AB_2 monomers. In this case, the LC phases may be formed on the molecular level on the subnanometer length scale.[27−30] However, introducing rodlike or disklike groups into dendrimers and hyperbranched polymers to form LC phases had been a challenging task because the incomparable geometric shapes of the molecules in the two different length scales (subnamometer and namometer). Other dendrimers and hyperbranched polymers exhibiting LC behaviors have also been reported including a series of carbosilane-based LC dendrimers,[31,32] lyotropic LC hyperbranched poltamides,[33] ferrocene-containing LC dendrimers,[34,35] and ferroelectric LC dendrimers and hyperbranched polymers.[36,37]

In this publication, we focus on a series of hyperbranched polynorbornenes having second generation LC monodendrons as side groups with a different degree of polymerization (*n*). Recently, detailed structural characterization of the second generation monodendrons, the building block of this polymer, indicates the existence of multiple LC phase transitions.[38] In the hyperbranched polynorbornenes, we find that, except in

[†] The University of Akron.
[‡] University of Pennsylvania.
[§] University of Sheffield.
* To whom correspondence should be addressed. E-mail: scheng@uakron.edu.

10.1021/ma0209895 CCC: $22.00
Published on Web 11/07/2002

Scheme 1. Dendritic Side-Chain Liquid-Crystalline Polymers DPNB(*n*)

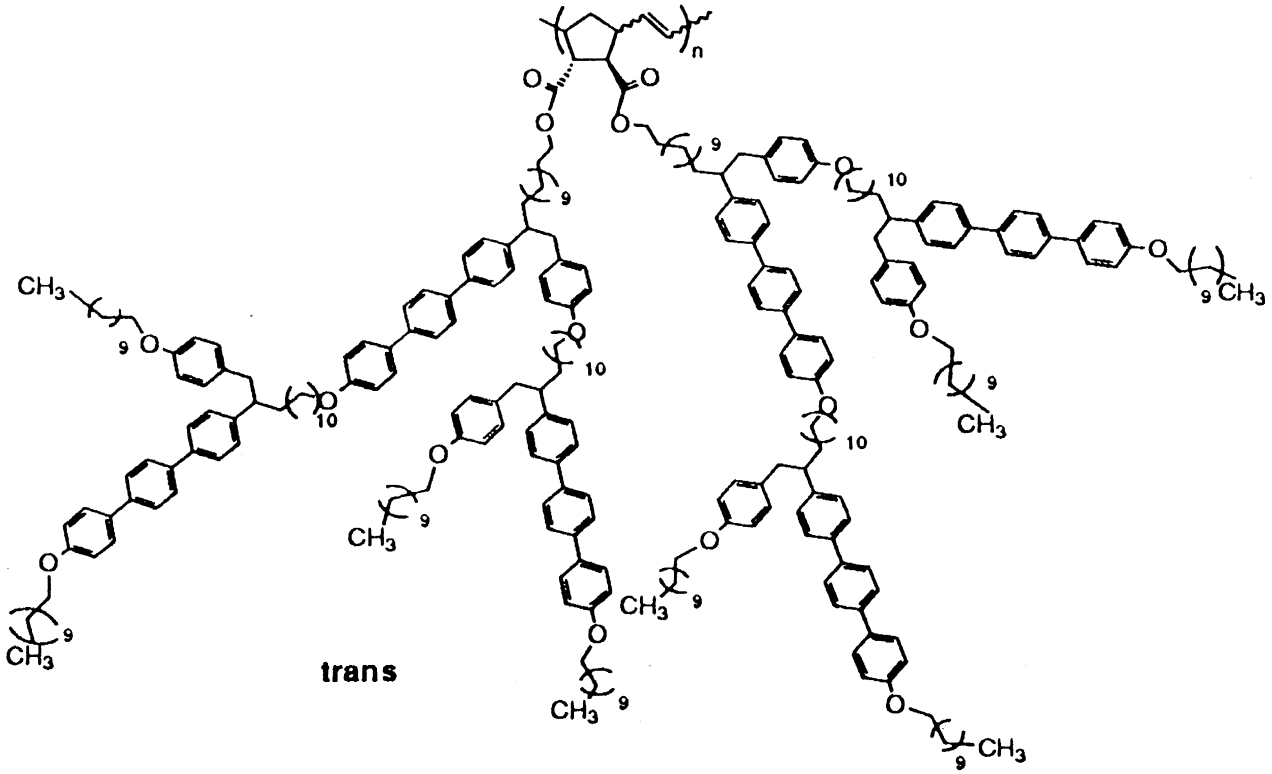

the nematic (N) phase, all other LC phases are formed in both the nanometer and subnanometer length scales, indicating that these phases are constructed by combinations of molecular and supramolecular structures. Their interrelationships are also discussed.

Experimental Section

Material Synthesis. A second generation monodendron (G_2NB) was synthesized via a divergent approach based on the conformationally flexible AB_2 mesogenic monomer, 13-hydroxy-1-(4-hydroxyphenyl)-2-(4-hydroxy-4″-*p*-terphenylyl)-tridecane building block.[27−30] The dendritic mesogenic norbornene was polymerized by ring-opening metathesis polymerization using $RuCl_2(=CHPh)(Pcy_3)_2$ as an initiator in dry CH_2Cl_2 at room temperature to form hyperbranched polynorbornenes. After the polymerization, the living polymers were quenched with ethyl vinyl ether. The detailed synthetic route has been previously published.[27−30] The chemical structure is shown in Scheme 1 [abbreviated as DPNB(*n*)]. The polydispesity of this series of polymer ranged between 1.09 and 1.29.

Equipment and Experiments. Differential scanning calorimetry (DSC) experiments were performed on a Perkin-Elmer DSC-7 equipped with a cooling apparatus to study the thermal transition behaviors of DPNB(*n*). The temperature and heat flow were calibrated using standard materials (indium and tin) at different cooling and heating rates between 1 and 40 °C/min under a dry nitrogen atmosphere. The cooling experiment was always performed first in order to eliminate the thermal history, followed by a heating experiment at a rate equal to the prior cooling rate. The temperature range used in this study was between 120 °C (20 °C above the isotropization temperature) and 15 °C (33 °C below the glass transition temperature of T_g = 48 °C). The onset transition temperatures were employed from both cooling at the high-temperature side and heating at the low-temperature side of the DSC diagrams. When isothermal experiments were conducted, the sample was cooled at 10 °C/min to a fixed temperature between 55 and 62 °C from the isotropic melt (I). The sample was kept at the isothermal temperature for different periods of time. It was then heated to 120 °C with or without prior cooling to below the T_g.

One-dimensional (1D) wide-angle X-ray diffraction (WAXD) powder experiments were carried out on a Rigaku 12 kW rotating anode generator (Cu Kα, λ = 0.154 nm) equipped with a diffractometer (radius of 185 mm). The X-ray beam was line-focused and monochromatized using a graphite crystal. The reflection peak positions and widths were calibrated with silicon crystals of known crystal size for the high-angle region ($2\theta > 15°$) and silver behenate for the low-angle region ($2\theta < 15°$). The range of the 2θ angle scanned was 1.5°−35°. A hot stage was built in the diffractometer to study the phase transitions. The heating and cooling experiments were conducted in the following way. During the scanning (at a rate of 10°/min in WAXD), the sample was set in the isothermal mode. As soon as the scan was finished, the samples were cooled or heated at a rate of 1 °C/min. Background scattering was subtracted from the sample's WAXD patterns. 1D small-angle X-ray scattering (SAXS) experiments at different temperatures were carried out at the synchrotron beamline X27C at the Brookhaven National Laboratory. The wavelength of the X-ray beam used was 0.1307 nm. A positional sensitive detector was used to record the SAXS data. The zero pixel was calibrated using a duck tendon, and the scattering vector q ($q = 4\pi \sin\theta/\lambda$, where λ is the wavelength of synchrotron X-ray beam and θ is the scattering angle) was calibrated by silver behenate. Measurements were performed on a customized two-chamber hot stage at different temperatures with experimental error controlled to be within ±0.5 °C.

Fibers were spun at 75 °C in the LC phase. Isothermal annealing processes were conducted on the fibers at different temperatures for prolonged periods of time in a fixed fiber length and subsequently quenched to the room temperature for phase structural determination. 2D WAXD fiber patterns were obtained from a Rigaku automated X-ray imaging system with an 18 kW rotating anode generator (Cu Kα). The calibration was identical to the 1D WAXD experiments previously reported. Air scattering was subtracted from the sample patterns.

Polarized light microscopy (PLM) experiments were performed on an Olympus HB-2 PLM coupled with a Mettler FP-90 hot stage to examine the phase morphology and LC defects. The temperature of the hot stage was calibrated with standard materials. Film samples can be prepared by pressing small

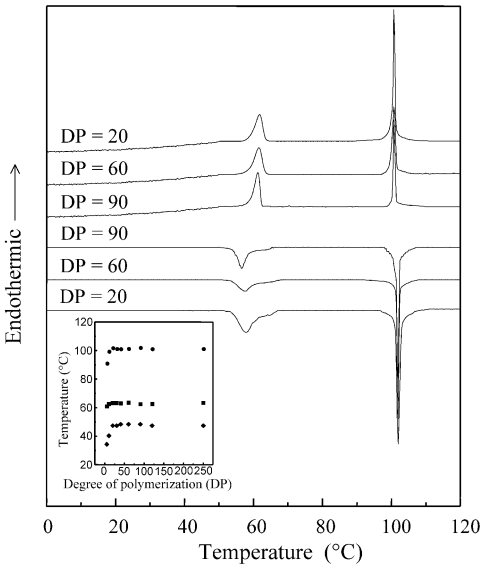

Figure 1. Two sets of DSC cooling and subsequent heating diagrams of DPNB(*n*) with different *n* of 20, 60, and 90 at a rate of 2.5 °C/min. The inset shows the transition temperature dependences upon the degree of polymerization (*n*).

amounts of samples between two glass slides in the I, and the thickness was ~10 μm. Mechanical shear was also applied on the film samples to identify the low ordered LC phase. A transmission electron microscope (TEM, JEOL 1200 EX II) was used to observe the morphology and provide structural information with an accelerating voltage of 120 kV. DPNB(*n*) samples were first dissolved in CH_2Cl_2 with 0.01% concentration and then cast onto a carbon-coated cover glass. The thickness of the resulting film was less than 30 nm. These films were subsequently annealed to grow larger size single domains. Hydrofluoric acid was used to dissolve the glass slide. Then, the acid was washed out by floating the samples on the surface of distilled water. The samples were then picked up using Cu grids, shadowed with carbon and platinum. Calibration of the electron diffraction (ED) in TEM experiments was carried out using TlCl for *d* spacing values smaller than 0.384 nm.

Results and Discussion

Thermal Properties of the Phase Transitions. Figure 1 shows two sets of DSC cooling and subsequent heating diagrams at a rate of 2.5 °C/min for DPNB(*n*) with different degrees of polymerization ($n = 20-90$). An initial review of Figure 1 suggests a similarity of the transition sequence among these samples. The inset of Figure 1 illustrates functions of the phase transition temperatures with the degree of polymerization. It is evident that beyond $n \geq 20$ all of the transition temperatures and heats of transitions become independent of *n*. These results are comparable to those reported for the *n* dependence of side chain LC polymers with different backbones such as polysiloxanes, polymethacrylates, polyacrylates, and poly(vinyl ether)s.[39] A DPNB(40) is thus chosen to investigate the phase transition behaviors and their corresponding structural changes.

Figure 2 shows two sets of DSC cooling and subsequent heating thermal diagrams of DPNB(40) at different rates between 1 to 40 °C/min. In the entire cooling temperature range from 120 to 15 °C, one apparent exothermic process at ~102 °C can be observed at different cooling rates. The onset transition temperature (101.7 °C) and the heat of transition (4.7 J/g) of this exothermic process are almost cooling-rate-independent.

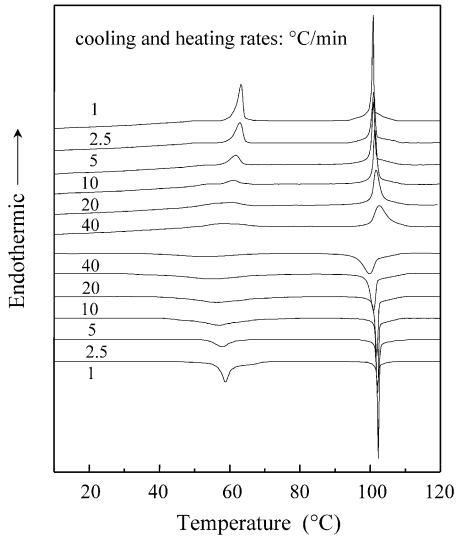

Figure 2. Two sets of DSC cooling and subsequent heating diagrams of DPNB(40) at different rates between 1 and 40 °C/min.

However, if we exam the DSC diagrams in Figures 1 and 2 carefully, it seems that this exothermic process is attributed to two overlapped transitions—narrow and broad. The transition peak temperatures of these two processes are close to one another (~2 °C difference), and the ratio between these two heats of transitions is roughly 2:1 (the narrow peak vs the broad peak) at cooling and heating rates of 1 °C/min. Both transitions may be associated with formations of low ordered LC phase structures (see below).

In the low-temperature region between 55 and 70 °C, broad exothermic processes are observed when the cooling rates are slower than 10 °C/min. At a cooling rate of 1 °C/min, the overall heat of transition is 1.6 J/g. With increasing cooling rate the width of the peak broadens, and the onset transition temperature and the heat of transition decrease. Above a cooling rate of 10 °C/min, the transition is so broad that a precise determination is not possible. This may be due to the fact that this exothermic process is close to the T_g of the polymer (48 °C).

During heating, as shown in Figure 2, the onset transition temperature in the high-temperature region is at 99.8 °C with a heat of transition of 4.6 J/g. It has little heating rate dependence (~0.8 °C). Again, this endothermic process seems to involve two transition processes—narrow and broad. Furthermore, the fact that the onset transition temperature during heating is lower than that during cooling is also an indication that more than one transition process is involved.[40-42] On the other hand, the endotherm in the low-temperature region is relatively broad (~63 °C). At a heating rate of 1 °C/min, the overall heat of transition is 1.6 J/g. Above the heating rate of 10 °C/min, again, the heat of transition cannot be precisely determined. During cooling at 1 °C/min, two exothermic processes can be identified. The first process is at 65 °C. Before this first process is fully developed, a second process begins at relatively low temperatures (see Figure 2).

To understand thermodynamic stability of these two phases, isothermal experiments in the vicinity of this temperature region are carried out. Figure 3 shows the DSC heating diagrams of DPNB(40) after the samples were isothermally kept at 62 °C for different periods of

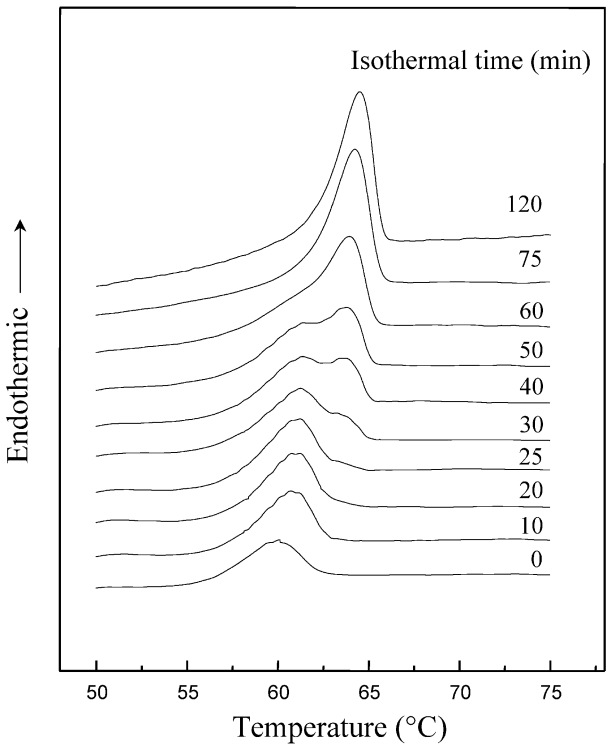

Figure 3. Set of DSC heating diagrams at 2.5 °C/min after the sample was isothermally kept at 62 °C for different times.

time and then cooled to below T_g. During the first 10 min, only one endothermic process exists. This process is formed during cooling of the sample after isothermal experiments because the entire endothermic process measured during heating is below the isothermal temperature of 62 °C and the heat of transition is 0.65 J/g. DSC diagrams recorded by direct heating without cooling after the isothermal experiment at 62 °C for 10 min does not show any endothermic transition in this temperature region. However, after kept isothermally for 10 min, another transition process appears, and this endotherm is formed during the isothermal experiments at 62 °C. With increasing the isothermal time, the growth of this endothermic process takes over the first process formed during cooling. After 120 min, the second endotherm dominates the whole endothermic process. This suggests that the first endotherm appearing at ~60 °C represents a phase which may be monotropic with respect to the second endotherm at ~63 °C. The second endotherm is gradually developed during the isothermal experiments (see below).[43,44] If the sample is annealed at slightly lower temperature of 60 or 61 °C, some differences of the transition behaviors can be observed. The first endothermic process formed during cooling after being isothermally kept at 62 °C for 10 min can now be partially developed during the isothermal experiments. The isothermal time for the full development of the second endotherm is also shortened.

Although DSC experiments are sensitive to transition processes that are associated with absorbing and releasing heats, they do not provide structural information in identifying the phase structures. Structural sensitive techniques such as WAXD, SAXS, and ED experiments need to be utilized.

Phase Structural Evolutions. Figure 4 shows a sets of 1D WAXD patterns for DPNB(40) at different temperatures upon slow and stepwise cooling. Combined with the DSC results performed at the same cooling and heating rates, the phase structural evolutions can be recognized. In Figure 4, when the temperature reaches 100 °C during cooling, a sharp Bragg reflection at $2\theta = 1.65°$ (d spacing of 5.35 nm) appears in the low-angle region, which corresponds to the exothermic transition at 102 °C in the DSC cooling experiments. Generally, this is recognized as layer diffraction. A diffuse scattering halo at around $2\theta \cong 20°$ is also observed. This is characteristic of the average distance among the chains in lateral packing, and it represents a liquidlike short-range order. Therefore, this phase should be a low ordered smectic (S) phase. Continuously cooling the sample to below 63 °C, corresponding to the low-temperature broad exothermic process observed in DSC cooling experiments, exhibits a sudden shift of the sharp Bragg reflection from $2\theta = 1.65°$ to 2° (d spacing of 4.42 nm) in the low-angle region. Note that in SAXS experiments a reflection at $2\theta = 1°$ (the d spacing of 8.84 nm) is seen (see below). This spacing is twice that of the reflection at $2\theta = 2°$, indicting that the reflection at $2\theta = 2°$ is of the second order. A new Bragg reflection also appears at $2\theta = 19.7°$ (d spacing of 0.45 nm), indicating the existence of the ordered chain lateral packing. This phase is closely associated with a highly ordered LC phase.

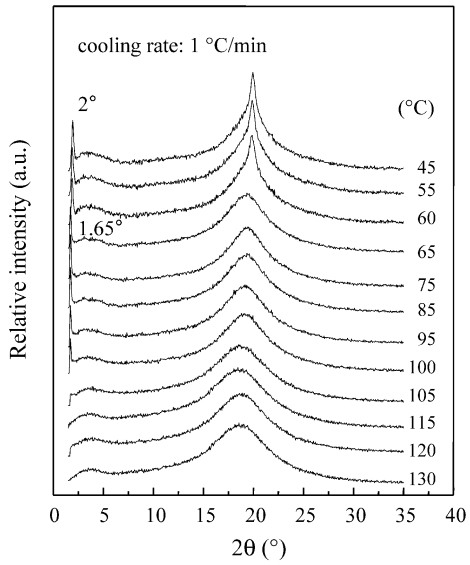

Figure 4. Set of 1D WAXD patterns at different temperature during cooling at a slow rate (see text).

Upon heating, all the structural changes obtained occur in a reversed sequence as the structural evolution during cooling. Both cooling and heating 1D WAXD patterns (see Figure 4) do not provide structural information on the possible monotropic phase which melts at ~60 °C because when the cooling experiment is slow (here, much slower than 1 °C/min), the highly ordered LC phase cannot be bypassed. To detect this phase, an isothermal WAXD experiment is required. Figure 5 shows a set of 1D WAXD patterns for DPNB(40) recorded during isothermal experiments at 62 °C for different periods of time and then subsequently heated to 80 °C at a slow stepwise heating. The first WAXD 2θ scan in this figure was performed as soon as the sample temperature reaches 62 °C after it cooled from the I at a rate of 10 °C/min. A sharp reflection at $2\theta = 1.8°$ (d spacing of 4.90 nm) in the low-angle region and a diffused scattering halo at a $2\theta \cong 20°$ in the wide-angle region are detected. This is a new phase structure which is attributed to the possible monotropic phase, and it

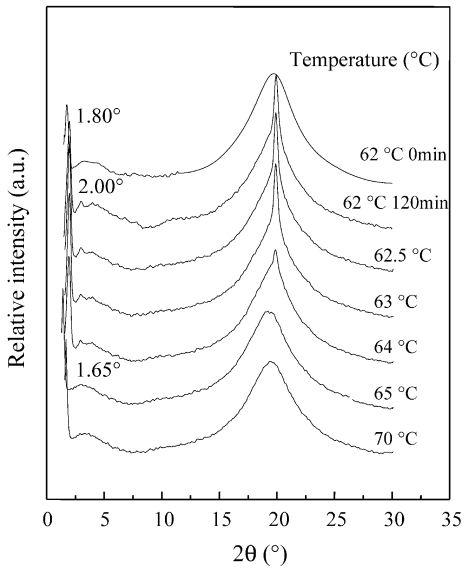

Figure 5. Set of 1D WAXD patterns for DPNB(40) isothermally kept at 62 °C at 0 and 120 min after the sample was cooled from 120 °C at a 10 °C/min. Subsequently, the sample was heated to 70 °C at 1 °C/min.

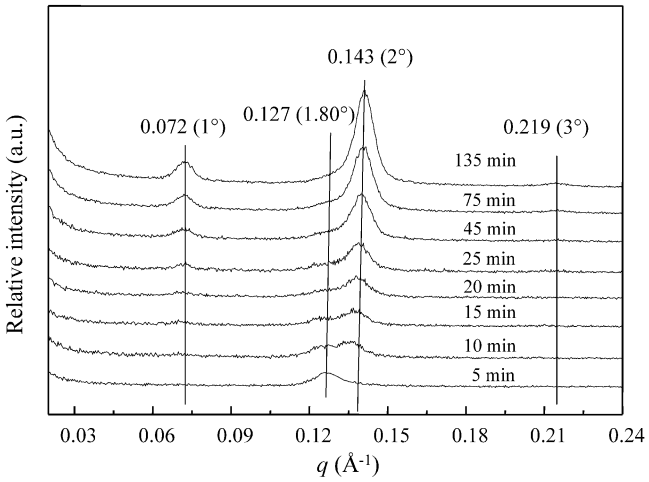

Figure 6. Set of 1D SAXS patterns for DPNB(40) isothermally kept at 62 °C at different times (the degrees have been converted to the wavelength of the Cu X-ray generator).

may be characterized as a low ordered S phase. After annealing the sample at 62 °C for 120 min, the layer reflection at $2\theta = 1.8°$ shifts back to $2\theta = 2°$. A Bragg reflection at $2\theta = 19.7°$ is also seen. This is the highly ordered S phase observed during slow cooling in WAXD. Therefore, this result indicates a transformation of this low order LC S phase to the stable, highly ordered S phase. Subsequent heating of this annealed sample leads to $2\theta = 1.65°$ when the temperature reaches 65 °C.

To understand the phase transformations which are characterized by the reflection changes in the low-angle region, synchrotron 1D SAXS isothermal experiments were performed. The sample thermal history is identical to the isothermal procedure used in DSC (Figure 3) and WAXD (Figure 5). As shown in Figure 6, at the early stage of the isothermal experiment, a Bragg reflection of $2\theta = 1.80°$ is observed, identical to the possible monotropic LC S-phase structure. After 10 min, a series of reflections start to appear which represent the highly ordered LC phase that develops with increasing time. This SAXS isothermal experiment thus also demonstrates the existence of this possible monotropic LC S phase. Namely, the transition temperature of this phase is lower than that of the highly ordered LC phase.[43,44] Moreover, Figure 6 shows that the high ordered LC phase possesses the first-, second-, and even third-order reflections at $2\theta = 1.0°$, 2.0°, and 3.0°. The intensity of the second-order reflections is stronger than that of the first-order reflections. However, the low ordered S phases exhibit only the first-order reflections at $2\theta = 1.65°$ and 1.80°. This reveals the layer ordered correlation differences among these phases.

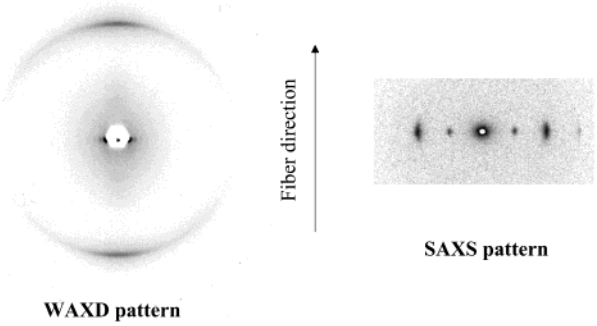

Figure 7. WAXD fiber pattern for DPNB(40) for the fiber spun at 75 °C and annealed at 55 °C for 2 days in order to fully develop the S_B^h phase.

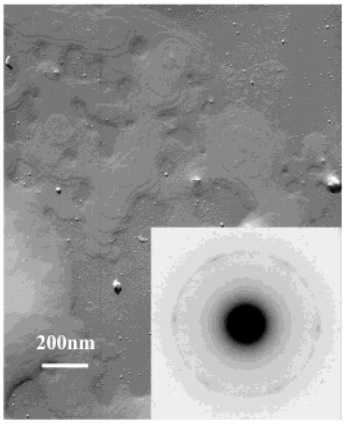

Figure 8. TEM morphological observation of flat-on lamellae and an ED pattern of the [00*l*] zone (in the inset).

Identification of the Highly Ordered LC Phase. Figure 7 shows DPNB(40) fiber patterns obtained in synchrotron 2D WAXD and SAXS experiments. The fibers were spun at 75 °C and annealed at 55 °C for 2 days. Three reflections on the equator in the SAXS pattern exhibit a ratio of 1:2:3 for their *q* values, indicating a presence of the layer structure. The layer spacing is 8.84 nm based on the calculation of the first-order reflections. A possible reason that the intensity of the second-order reflections is stronger than that of the first-order reflections may be associated with the arrangement of the LC monodendrons, a scenario similar to the case of the second generation monodendron of G_2NB. Note that G_2NB is the side group of DPNB(*n*).[38] The LC G_2NBs adopt the anti conformation when they are packed in the layered structure. The branch ends are accumulated not only at the layer boundaries but also at the center of the layers. This results in an additional electron density periodicity difference at the halfway across the layer profile. Only a partial extinction of the first-order reflection can be achieved, causing the intensity of second-order reflection to be stronger than that of the first-order reflection in

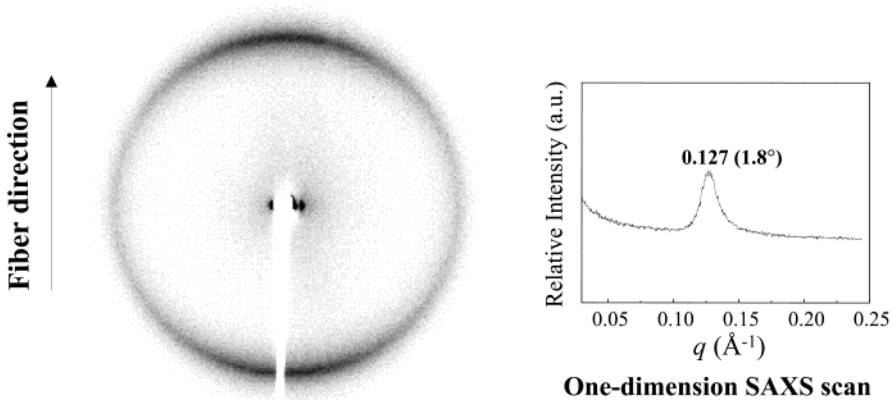

Figure 9. WAXD fiber pattern for DPNB(40) for the fiber spun at 75 °C and immediately quenched to liquid nitrogen without annealing in order to develop the S_A^m phase. A one-dimensional SAXS scan along the equatorial is also included, and a $2\theta = 1.8°$ at the low angle region is observed.

the low-angle region.[28,38] In the DPNB(40) case, the backbones may also be included in the layers. However, detailed understanding of the backbone and side group arrangements in this highly ordered LC phase needs further study using computer simulations. A pair of sharp reflections at $2\theta = 19.7°$ is found on the meridian, indicating the ordered lateral chain packing. Analysis of the X-ray data suggests that the mesogens are arranged parallel to the layer normal, meaning that it is perpendicular to the fiber direction.

Evidence of this ordered lateral chain packing within the layers is also provided by the ED pattern in TEM. The sample was prepared from dilute solution and annealed at 48 °C for 6 days. Flat-on lamellae are observed in TEM as shown in Figure 8, and the [00*l*] ED pattern is the inset of this figure. The ED pattern consists of six diffraction spots with a *d* spacing of 0.45 nm. This suggests a 2D hexagonal lattice having $a = 0.52$ nm and $\gamma = 120°$, which corresponds to the sharp diffraction at $2\theta = 19.7°$ in the powder and fiber WAXD patterns. Because the intensity of these spots is weak and higher-order diffractions are not observed, long-range positional order of this 2D hexagonal packing may not exist within the layers. On the basis of these WAXD, SAXS, and ED results, this highly ordered LC phase can be identified as the hexatic B (S_B^h) phase having a layer spacing of 8.84 nm.[45,46]

Generally speaking, the layer spacing in a S phase is represented by one chemical repeat unit, which is the sum of the length of one spacer and one mesogen. In the case of DPNB(40), the layer *d* spacing is 8.84 nm, which is much larger than the length of the chemical repeat unit. We believe that the layer structure in the S_B^h phase of DPNB(*n*) is constructed via the whole G_2NB monodendron side groups in the polymer. This is a supramolecular structure on the nanometer scale. On the other hand, the DPNBs also possess the LC mesogens in the side groups, which forms a 2D hexagonal array on a subnanometer scale. Therefore, the S_B^h phase actually consists of both the nanometer and the subnanometer structures.

Since the 2D WAXD fiber pattern shown in Figure 7 exhibits unusual orientations, i.e., the layer normal is perpendicular to the fiber direction and the lateral packing direction is parallel to the fiber direction, the chain conformations in the formation of this LC S_B^h phase adopted by DPNB(40) in the fibers need further discussion. When the fibers were spun, the longest contour length of the macromolecules should be a principal contribution to entangling them together. This longest contour length of DPNB(40) must be the backbone length coupled with two long branches of the monodendrons at the two ends of the backbones. Therefore, in the fibers, the backbones have to be parallel to the fiber direction, and the LC mesogens form the hexagonal lateral packing structures of which the lateral packing direction is parallel to fiber direction; i.e., the mesogen direction is perpendicular to the fiber direction. Since the fibers were spun in the S phase (at 75 °C, see below), it is possible that this unusual orientation is due to the alignment of the S layer planes along the flow direction during the spinning of the fibers. This is similar to the cases recently reported in a series of LC copoly(ester imide)s[47,48] and other LC polymers and oligomers.[49−51]

Identification of the Low Ordered LC Phase. From the DSC, 1D WAXD, and SAXS results, there exist two low order LC S phases. The first one may be monotropic which melts at a temperature of ∼60 °C (Figures 3, 5, and 6). To further identify this phase structure, quenched as-spun fibers, which were spun at 75 °C without any annealing, are used to obtain a 2D fiber pattern of DPNB(40) as shown in Figure 9. A pair of sharp Bragg diffraction spots at $2\theta = 1.8°$ is observed on the equator. Only a pair of diffuse scattering arcs at $2\theta \cong 20°$ on the meridian is seen, indicating that the lateral chain packing within the layers is in liquidlike short-range order. Since the LC mesogen lateral packing direction is perpendicular to the layer normal, this phase is identified as an S_A^m phase with a layer spacing of 4.90 nm.

The second, stable LC S phase has been identified in a temperature region between 65 and 100 °C based on the DSC, 1D WAXD, and SAXS results. The fiber of DPNB(40) was spun at 75 °C and then annealed at 70 °C for 10 h before they were quenched to room temperature. The 2D WAXD and SAXS fiber patterns are very similar to those in Figure 9. Only one difference is that a pair of sharp spots at $2\theta = 1.65°$ are observed on the equator, which represents the layer spacing of 5.35 nm. Therefore, this phase can also be identified as a S_A phase. The only difference between these two S_A phases is that the S_A^m phase at ∼60 °C possesses a smaller layer spacing (4.90 vs 5.35 nm).

In addition to these three phases, morphological observation of DPNB(40) in PLM reveals the existence

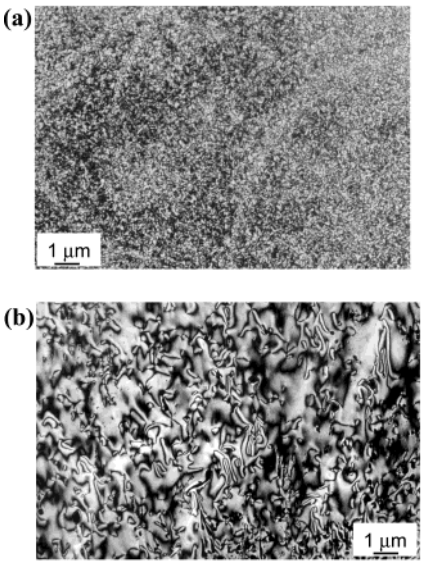

Figure 10. PLM morphological observations: (a) a fine, grainy texture is observed at 100.5 °C; (b) after annealing the sample at 100.5 °C for 1 h, a typical schlieren texture of the N phase is observed.

of a N phase near the isotropization temperature. Note that the N phase can only be characterized by a small, sudden shift of the *d* spacing of the scattering halo in the wide-angle region of the 1D WAXD patterns, indicating a change in the average distances between the laterally chain packing. This method has been used to identify low ordered LC phase transitions in several main-chain LC polymers.[52−57] Here, however, it is difficult to use this method since the temperature window of the N phase is too small (less than 2 °C). Therefore, the PLM becomes the major characterization method in identifying the N phase. Figure 10a,b shows the PLM images when the temperature reaches 100.5 °C during cooling and annealed there for 1 h. Observations of two and four dark brushes emanate from point singularities (Figure 10b), revealing the typical feature of the N phase.

The existence of this N phase can also be verified by the observation of two transition processes in the vicinity of 102 °C in the DSC results of Figures 1 and 2. The heat of transition of the broad transition process is estimated to be 1.6 J/g. Note that the N phase has been identified in the G_2NB monodendrons, which are the side groups of DPNB(*n*), and its heat of transition is also 1.6 J/g.[28,38] Thus, it is possible that the broad exothermic transition is the I → N phase transition and the narrow exothermic transition is the N → S_A phase transition during cooling. Both transitions can also be recognized during heating.

Interrelationships between Nanometer and Subnanometer Structures. It is interesting that in DPNB(40) there are a series of phases which are constructed on different length scales during cooling and heating. The sequences of the phase transitions are

$$\text{during cooling:}\quad I \rightarrow N \rightarrow S_A \rightarrow (S_A^m) \rightarrow S_B^h$$

$$\text{during heating:}\quad S_B^h \rightarrow S_A \rightarrow N \rightarrow I$$

Among these phases, the N phase is formed via orientation order of the LC mesogens in the side groups on the subnanometer scale. The layer structures of both of the S_A and S_A^m phases are constructed on the nanometer scale in the supramolecular level, which are associated with the entire side groups rather than the mesogens in the side chains. Within the layers of these two phases, the mesogens retain the orientation order. On the other hand, the S_B^h phase has layer structure formed by the entire side groups on the nanomter scale, while the 2D hexagonal lateral packing on the subnanometer scale which is attributed to the mesogens in the side chains.

Recognition of the possible metastable S_A^m phase during cooling brings up an important issue. The transition between the S_A and S_A^m phases is purely attributed to the change in the nanometer layer structures, since these two phases possess identical orientation order within the layers but different layer spacings (and thus different phase densities). Therefore, this is a pure supramolecular structural transition. Thermodynamic properties of a supramolecular transition are generally associated with a cooperative dynamics such as in colloid crystals and diblock copolymers. This type of transitions commonly possesses a major entropy change and a relatively minor enthalpy change.[58] In the DPNB(40) case, this supramolecular transition can still be detected in DSC, indicating that although this transition is only represented by the layer spacing difference on the nanometer scale, it must also be associated with a change of cooperative interactions among the molecules.

The layer structure in the S_B^h phase can be formed from either the S_A or the S_A^m phase. Although the layer spacings of the initial states of the S_A and the S_A^m are different (and thus density difference), the layer spacing of the final S_B^h phase is independent of the formation pathways although we expect that the formation kinetics may be different. It is speculated that this layer spacing change is triggered by the formation of the 2D hexagonal array of the mesogens in the LC monodendrons. Furthermore, in G_2NB the layer spacing of the S_B^h phase is 9.06 nm,[38] while in the S_B^h phase of DPNB(40), the layer spacing is 8.84 nm. The polynorbornene backbones thus slightly affect the layer spacing. On the other hand, the low ordered S phases in DPNB(40) are all in the S_A phases. In the case of G_2NB, the low ordered S phase is in the S_C phase. This can be explained by the fact that in DPNB(40) the backbones may limit the mobility of the mesogens within the supramolecular layers. Therefore, they will retain the relationship between the orientation of the mesogenic groups and the layer normal. This may not be the case in G_2NB fibers since the mesogenic groups may follow the stretch direction as long as they have enough mobility when the supramolecular layers still remains, indicating a disassociation of the cooperative mobility between the mesogenic groups and the supramolecular layer structures. Further investigation is, however, necessary in order to quantitatively understand these effects on the changes of these nanometer and subnanometer structures.

Conclusion

In summary, multiple phase transformations are identified in a polymer DPNB(40) based on DSC, WAXD and SAXS, PLM, and ED in TEM experimental results. Among these phases, the N phase is formed via mesogens in the monodendrons of the side chains. The layer structures in both of the S_A and S_A^m phase forma-

tions are attributed to the assembly on the nanometer length scale via reorganization of the entire side groups, while within the layers the orientation order of the mesogens in the subnanometer level is retained. Despite this fact, the S_B^h phase is constructed by the structures on of both the nanometer and subnanometer scales. The S_A^m phase is a possible metastable phase and monotropic with respect to the S_B^h phase. The different pathways of the phase transition sequence affect the formation the layer structures in these three S phases.

Acknowledgment. This work was supported by the National Science Foundation (DMR-9617030) and the Science and Technology Center for Advanced Liquid Crystal Optical Materials (ALCOM) at Kent State University, Case Western Reserve University, and the University of Akron (DMR-9157738).

References and Notes

(1) Flory, P. J. *J. Am. Chem. Soc.* **1941**, *63*, 3083; *J. Am. Chem. Soc.* **1952**, *74*, 2718.
(2) Flory, P. J. *J. Phys. Chem.* **1942**, *46*, 132; *J. Phys. Chem.* **1949**, *17*, 303.
(3) See for example: Buhleier, E.; Wehner, W.; Vögtle, F. *Synthesis* **1978**, *2*, 155.
(4) Denkewalter, R. G.; Kolc, J. F.; Lukasavage, W. J. U.S. Patent 4,410,688, 1979.
(5) Aharoni, S. M.; Crosby, C. R., III.; Walsh, E. K. *Macromolecules* **1982**, *15*, 1903.
(6) Kricheldorf, H. R.; Zang, Q.-Z.; Schwarz, G. *Polymer* **1982**, *23*, 1821.
(7) Maciejewski, M. *Macromol. Sci. Chem.* **1982**, *A17*, 689.
(8) Tomalia, D. A.; Baker, H.; Deward, J.; Hall, M.; Kallos, G.; Martin, S.; Roeck, J.; Ryder, J.; Smith, P. *Polym. J.* **1985**, *17*, 117.
(9) Tomalia, D. A.; Naylor, M.; Goddard, W. A., III *Angew. Chem., Int. Ed. Engl.* **1990**, *29*, 138.
(10) Yin, R.; Zhu, Y.; Tomalia, D. A. *J. Am. Chem. Soc.* **1998**, *120*, 2678.
(11) Newkome, G. R.; Yao, Z.-Q.; Baker, G. R.; Gupta, V. K. *J. Org. Chem.* **1985**, *50*, 2003.
(12) Hawker, C. J.; Fréchet, J. M. *J. Am. Chem. Soc.* **1990**, *112*, 7638.
(13) Miller, T. M.; Neenan, T. X. *Chem. Mater.* **1990**, *2*, 346l.
(14) Moore, J. S.; Xu, Z. *Macromolecules* **1991**, *24*, 5893.
(15) Fréchet, J. M. *Science* **1994**, *263*, 1710.
(16) Klopsch, R.; Franke, P.; Schlüter, A. D. *Chem.—Eur. J.* **1996**, *2*, 1330.
(17) Wooley, K. L.; Hawker, C. J.; Fréchet, J. M. *J. Am. Chem. Soc.* **1991**, *113*, 4252.
(18) Wooley, K. L.; Hawker, C. J.; Fréchet, J. M. *Angew. Chem., Int. Ed. Engl.* **1994**, *33*, 82.
(19) Labbe, G.; Forier, B.; Dehaen, W. *Chem. Commun.* **1996**, *18*, 2143.
(20) Kim, Y. M. *Adv. Mater.* **1992**, *4*, 764.
(21) Voit, B. I. *Acta Polym.* **1995**, *46*, 87.
(22) Percec, V.; Heck, J. A.; Tomazos, D.; Falkenberg, F.; Blackwell, H.; Ungar, G. *J. Chem. Soc., Perkin Trans. 1* **1993**, *22*, 2799.
(23) Percec, V.; Heck, J. A.; Tomazos, D.; Ungar, G. *J. Chem. Soc., Perkin Trans. 2* **1993**, *12*, 2381.
(24) Hudson, S. D.; Jung, H.-T.; Percec, V.; Cho, W.-D.; Johansson, G.; Ungar, G.; Balagurusamy, V. S. K. *Science* **1997**, *278*, 449.
(25) Balagurusamy, V. S. K.; Ungar, G.; Percec, V.; Johansson, G. *J. Am. Chem. Soc.* **1997**, *119*, 1539.
(26) Percec, V.; Ahn C.-H.; Ungar, G.; Yeardley, D. J. P.; Moller, M.; Sheiko, S. S. *Nature (London)* **1998**, *391*, 161.
(27) Percec, V.; Chu, P.; Kawasumi, M. *Macromolecules* **1994**, *27*, 4441.
(28) Percec, V.; Chu, P.; Ungar, G.; Zhou, J. *J. Am. Chem. Soc.* **1995**, *117*, 11441.
(29) Pervec, V.; Chu, P. *Polym. Prepr. (Am. Chem. Soc., Div. Polym. Chem.)* **1995**, *36*, 743.
(30) Li, J. F.; Crandall, K. A.; Chu, P. W.; Percec, V.; Petschek, R. G.; Rosenblatt, C. *Macromolecules* **1996**, *29*, 7813.
(31) Lorenz, K.; Hotler, D.; Stuhn, B.; Mulhaupt, R.; Frey, H. A. *Adv. Mater.* **1996**, *8*, 414.
(32) Ponomarenko, S. A.; Rebrov, E. A.; Bobrovsky, A. Y.; Boiko, N. I.; Muzafarov, A. M.; Shibaev, V. P. *Liq. Cryst.* **1996**, *21*, 1.
(33) Kim, Y. H. *J. Am. Chem. Soc.* **1992**, *114*, 4947.
(34) Deschenaux, R.; Serrano, E.; Levelut, A. M. *Chem. Commun.* **1997**, *16*, 1577.
(35) Dardel, B.; Deschenaux, R.; Even, M.; Serrano, E. *Macromolecules* **1999**, *32*, 5193.
(36) Bauer, S.; Fischer, H.; Ringsdorf, H. *Angew. Chem., Int. Ed. Engl.* **1993**, *32*, 1589.
(37) Busson, P.; Ihre, H.; Hult, A. *J. Am. Chem. Soc.* **1998**, *120*, 9070.
(38) Liu, Z.; Zhu, L.; Zhou, W.; Cheng, S. Z. D.; Percec, V.; Ungar, G. *Chem. Mater.* **2002**, *14*, 2384.
(39) Percec, V.; Pugh, C. *Side Chain Liquid Crystalline Polymers*; McArdle, C. B., Ed.; Chapman and Hall: New York, 1989.
(40) Ge, J. J.; Honigfort, P. S.; Ho R.-M.; Wang, S.-Y.; Harris, F. W.; Cheng, S. Z. D. *Macromol. Chem. Phys.* **1999**, *200*, 31.
(41) Kim, G.-H.; Pugh, C.; Cheng, S. Z. D. *Macromolecules* **2000**, *33*, 8983.
(42) Kim, G.-H.; Jin, S.; Pugh, C.; Cheng, S. Z. D. *J. Polym. Sci., Polym. Phys. Ed.* **2001**, *39*, 3029.
(43) Keller, A.; Cheng, S. Z. D. *Polymer* **1998**, *39*, 4461.
(44) Cheng, S. Z. D.; Keller, A. *Annu. Rev. Mater. Sci.* **1998**, *28*, 533.
(45) Gray, G. W.; Goodby, J. W. G. *Smectic Liquid Crystals: Textures and Structures*; Leonard Hill: London, 1984.
(46) Pershan, P. S. *Structure of Liquid Crystal Phases*; World Scientific: Singapore, 1988.
(47) Leland, M.; Wu, Z.; Chhajer, M.; Ho, R.-M.; Cheng, S. Z. D.; Keller, A.; Kricheldorf, H. R. *Macromolecules* **1997**, *30*, 5249.
(48) Leland, M.; Wu, Z.; Ho, R.-M.; Cheng, S. Z. D.; Kricheldorf, H. R. *Macromolecules* **1998**, *31*, 22.
(49) Romouribe, A.; Windle, A. H. *Macromolecules* **1993**, *26*, 7100.
(50) Li, C. Y.; Ge, J. J.; Bai, F.; Zhang, J. Z.; Calhoun, B. H.; Chien, L. C.; Harris, F. W.; Cheng, S. Z. D. *Polymer* **2000**, *41*, 8953.
(51) Ungar, G.; Zhou, J.; Percec, V.; Chu, P. *Makromol. Chem. Makromol. Symp.* **1995**, *98*, 951.
(52) Ungar, G.; Feijoo, J. L.; Percec, V.; Tound, R. *Macromolecules* **1991**, *24*, 953.
(53) Yandrisits, M. A.; Cheng, S. Z. D.; Zhang, A.-Q.; Cheng, J.; Wunderlich, B.; Percec, V. *Macromolecules* **1992**, *25*, 2112.
(54) Pardey, R.; Zhang, A.; Gabori, P. A.; Harris, F. W.; Cheng, S. Z. D.; Adduci, J.; Facinelli, J. V.; Lenz, R. W. *Macromolecules* **1992**, *25*, 5060.
(55) Pardey, R.; Shen, D.; Gabori, P. A.; Harris, F. W.; Cheng, S. Z. D.; Adduci, J.; Facinelli, J. V.; Lenz, R. W. *Macromolecules* **1993**, *26*, 3687.
(56) Yoon, Y.; Zhang, A.; Ho, R.-M.; Cheng, S. Z. D.; Percec, V.; Chu, P. *Macromolecules* **1996**, *29*, 294.
(57) Yoon, Y.; Ho, R.-M.; Moon, B.-S.; Kim, D.; McCreight, K. W.; Li, F.; Harris, F. W.; Cheng, S. Z. D.; Percec, V.; Chu, P. *Macromolecules* **1996**, *29*, 3421.
(58) Tu, H.; Wan, X.; Liu, Y.; Chen, X.; Zhang, D.; Zhou, Q.-F.; Ge, J. J.; Shen, Z.; Jin, S.; Cheng, S. Z. D. *Macromolecules* **2000**, *33*, 6315.

MA0209895